APL Materials

The growth and phase distribution of ultrathin SnTe on graphene

Cite as: APL Mater. **7**, 041102 (2019); https://doi.org/10.1063/1.5091546
Submitted: 03 February 2019 . Accepted: 08 March 2019 . Published Online: 02 April 2019

Kai Chang, and Stuart S. P. Parkin

The growth and phase distribution of ultrathin SnTe on graphene

Cite as: APL Mater. 7, 041102 (2019); doi: 10.1063/1.5091546
Submitted: 3 February 2019 • Accepted: 8 March 2019 •
Published Online: 2 April 2019

Kai Chang and Stuart S. P. Parkin[a)]

AFFILIATIONS

Max-Planck Institute of Microstructure Physics, Halle 06120, Germany

[a)]Email: stuart.parkin@mpi-halle.mpg.de

ABSTRACT

Recently, a monolayer of SnTe was discovered to be a two-dimensional ferroelectric with an in-plane polarization, and, most dramatically, it exhibits a significant enhancement of the ferroelectric phase transition temperature compared to its bulk counterpart. This phenomenon is due to a structural phase transition from bulk-like α/β-SnTe, a topological crystalline insulator, to layered γ-SnTe as the thickness is decreased to a few atomic layers. A detailed understanding of the growth mechanism and phase distribution of ultrathin SnTe films are of great interest for potential applications. Here, we report detailed studies of the molecular beam epitaxial growth and *in situ* scanning tunneling microscopy characterization of ultrathin SnTe films on graphene substrates. By varying the growth conditions, SnTe can be prepared as either a continuous film or in the form of large rectangular plates. The rate of nucleation of SnTe was found to be highly sensitive to the substrate temperature. The coexistence and competition between the β and γ phases formed at room temperature was studied, and the phase diagram with respect to the average thickness of SnTe and the substrate temperature during growth is drawn.

The discovery of two-dimensional (2D) ferroelectric materials in the past few years has opened a promising field for novel nanoscale non-volatile electronic devices.[1] Several 2D group-IV monochalcogenides, monolayer MX (M = Ge, Sn; X = S, Se), are predicted to possess robust in-plane piezoelectricity and ferroelectricity.[2–7] The ferroelectric transition temperatures (T_c) in some of these materials were predicted to be above room temperature.[4–7] Just as the monolayer transition metal dichalcogenides (TMDCs) can be viewed as graphene-like lattices with a staggered sublattice potential,[8] monolayer MX materials are akin to the staggered-lattice form of black phosphorus.[9] Inversion symmetry is broken both in the monolayer TMDCs as well as the MXs. However, as distinct from the TMDCs, the spontaneous polarization in monolayer MX can be tuned by applying an external electric field or stress,[7] which makes monolayer MX a promising platform for non-volatile memory devices. Bulk MX materials exhibit a layered structure (space group *Pnma*).[10] Each unit cell is composed of two monolayers, which are related to each other by a glide-mirror operation and each monolayer contains two atomic layers (ALs). In-plane spontaneous polarization emerges within each monolayer, while the coupling between the neighboring monolayers is antipolar, and hence no net polarization is shown in bulk MX materials. When the thickness is decreased to one monolayer (2 AL), the space group of the system reduces to non-centrosymmetric $Pmn2_1$, and a net polarization appears. In MX films with a thicknesses of $4n - 2$ AL (n = 1, 2, 3 . . .), a finite total polarization exists along the c axis of the crystal (in-plane "armchair" direction). While most theoretical predictions have been made for free-standing systems, it is still very challenging to prepare strain-free monolayer MX films and to characterize their polarization. Recent scanning tunneling microscopy (STM) experiments have revealed that monolayer SnTe films grown on graphene substrates show unexpectedly robust in-plane ferroelectricity with a T_c as high as 270 K,[11] much higher than that of the bulk material (T_c < 100 K).[12] Further studies have revealed that as the thickness decreases, the space group of the SnTe film transitions from $Fm\bar{3}m$ (above T_c, paraelectric, β phase) or $R3m$ (below T_c, ferroelectric, α phase) in bulk material to *Pmna* ($4n$ AL thick) or $Pmn2_1$ ($4n - 2$ AL thick) in nearly strain-free ultrathin films (layered γ phase).[13] Since the lattice structure and properties of γ-SnTe agree well with the predictions of ferroelectric MX monolayers, it becomes the first experimentally confirmed 2D ferroelectric material in this family. The spontaneous polarization of γ-SnTe is stable at room

temperature when the film is thicker than 2 AL,[11,13] making it potentially useful for applications. In films with thicknesses between 6 and 20 AL, the α/β and γ phases can coexist.[13] It is worth noting that bulk SnTe in the α or β phase and its isomorphic cousins $Pb_{1-x}Sn_xTe$ and $Pb_{1-x}Sn_xSe$ are topological crystalline insulators, which have band inversions in their electronic band structures and mirror symmetry protected gapless surface states with Dirac-cone shaped energy dispersionss.[14–17] Thus, controlling the thickness, topography, and the distribution of the different phases becomes an important topic for possible future applications. Here, we report a systematic study of the molecular beam epitaxial (MBE) growth of ultrathin SnTe films on graphene substrates, focused on the thickness-dependent structural phase transitions.

Graphene was chosen as the substrate in this study because of its very low surface energy (62 mJ/m^2),[18] which guarantees a van der Waals epitaxy that is not sensitive to lattice matching conditions, and its sufficient conductance, which is required for scanning tunneling microscopy (STM) measurements. Nitrogen doped Si-terminated 6H-SiC(0001) substrates (MaTecK, 2 mm × 10 mm × 0.33 mm) were used for the epitaxial growth of graphene layers. The substrate can be prepared using any of these three procedures: (i) annealing SiC in H_2/Ar mixed gas;[19] (ii) annealing SiC in an ultra-high vacuum (UHV) environment by passing direct current through the substrate, with the assistant of a Si flux;[20] (iii) flash annealing SiC in UHV by direct current heating.[21] The first method can create substrates with the most regular terraces and the least defect densities but requires *ex situ* annealing in a furnace before the substrate can be loaded into an MBE system. The third method has the least requirements concerning equipment but is relatively time-consuming. Thus, substrates used in this study were prepared with the second method. Specifically, a SiC substrate was first degassed at 500 °C until the chamber pressure returns to its base value (5×10^{-10} mbar) and then was annealed at 900 °C in a Si flux for 15 min to form a Si-rich 3 × 3 reconstruction on the surface. Finally, the substrate was annealed at 1400 °C for 10 min, during which the surface was covered by a monolayer or a bilayer of graphene. The substrate temperature was measured using an infrared pyrometer. The crystalline orientation of graphene formed in this way is rotated 30° from that of SiC(0001), as Figs. 1(c) and 1(f) show. The steps on the substrate generally follow the $\langle 11\bar{2}0 \rangle$ directions of SiC or the $\langle 01 \rangle$ directions of the SiC-(0001) surface. Some graphene wrinkles with heights of 2–3 nm can be occasionally seen on the substrates. SnTe molecules were evaporated from SnTe granules (Alfa Aesar, 99.999%) in a h-BN crucible at a temperature of 450 °C. The flux of SnTe was kept constant in all experiments. After deposition, the sample was transferred into an Omicron variable temperature (VT) STM without breaking the UHV environment. All the experiments were performed at room temperature. Pt/Ir tips calibrated on the Au(111) surface were used for STM measurements. For the statistical studies, a MATLAB code was used to count the areas of different thicknesses, semi-automatically.

Since all the data were collected at room temperature, only γ and β phases appear in the experiments, as Figs. 1(a) and 1(b) illustrate. The β phase transitions into the α phase at low temperatures. Reflection high energy electron diffraction (RHEED) patterns of SnTe samples display sharp stripes, indicating the growth of uniform films or large plates, as Figs. 1(c)–1(e) show. Four stripes from SnTe are visible in Fig. 1(e), whose distances from the zeroth stripe,

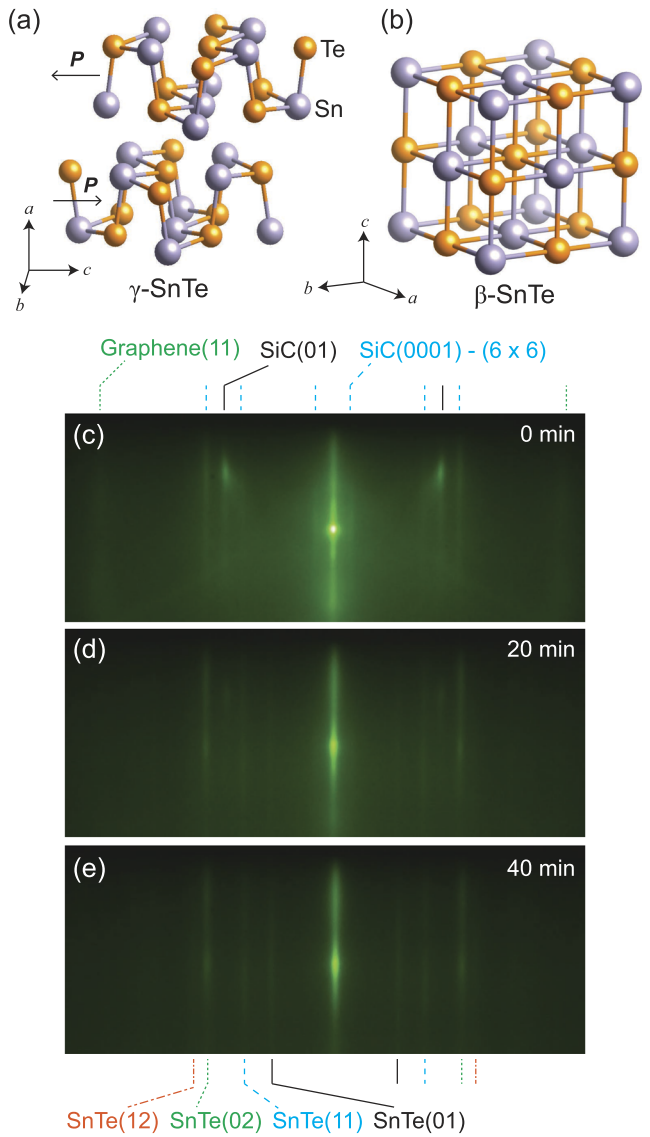

FIG. 1. [(a) and (b)] The lattice structures of SnTe in the γ phase (a) and the β phase (b). The arrows in (a) indicate the directions of spontaneous polarization within each monolayer. [(c)–(e)] RHEED patterns of a bare substrate (c); a SnTe sample with part of the substrate covered (d) and fully covered (e). Attributions of the RHEED stripes are indicated.

1.4 Å^{-1}, 2.0 Å^{-1}, 2.8 Å^{-1}, and 3.2 Å^{-1}, respectively, can be calculated by calibrating with the pattern from the substrate. Comparing with the reciprocal lattices of SnTe surfaces (lattice parameters b = 4.44 Å and c = 4.58 Å for γ-SnTe[11] and a = 4.47 Å for β-SnTe[22]), these stripes are attributed to the (01), (11), (02), (12) stripes of SnTe. The RHEED patterns imply a growth of uniform (100) surfaces for both β and γ phases but random in-plane crystalline orientation.

Because of the low surface energy of graphene substrates, the nucleation rate of SnTe on graphene is highly sensitive to the substrate temperature. Therefore, by varying the combination of substrate temperature, molecular flux rate, and growth time,

very different surface topographies can be obtained, such as standalone rectangular plates, continuous films in the γ phase, or a mixture of γ and β phases, as Figs. 2(b)–2(d) show. We will discuss the dependence of surface topology on growth conditions later.

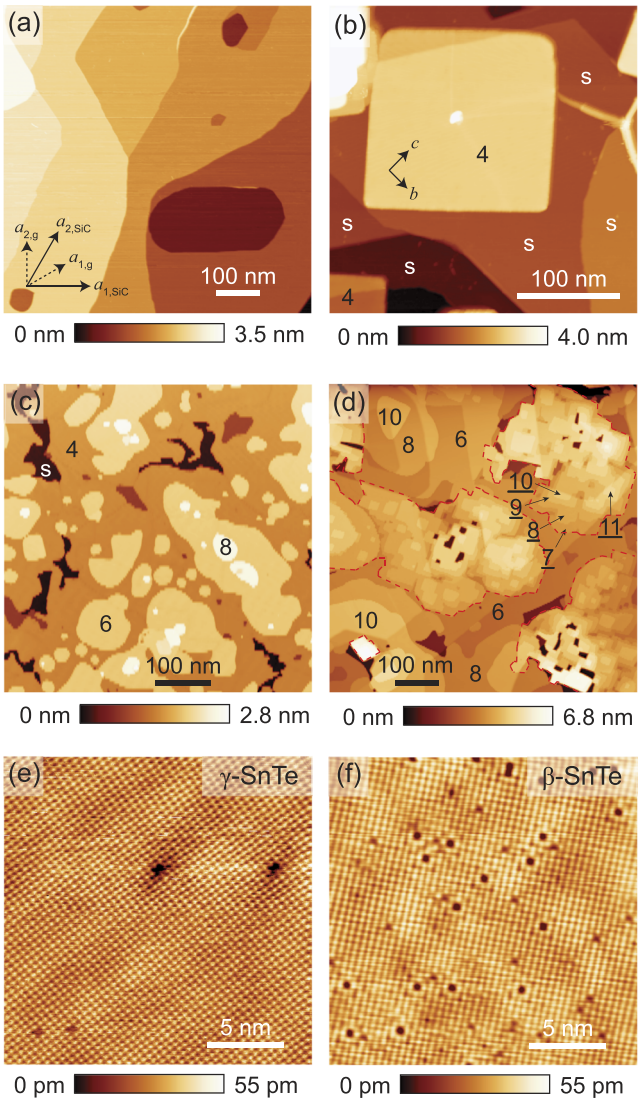

FIG. 2. (a) STM topographic image of the graphene substrate. The solid and dashed arrows indicate the directions of the lattice basis of the SiC(0001) surface and graphene, respectively. [(b)–(d)] Typical topography images of ultrathin SnTe films or plates for different growth conditions. (b) γ-SnTe plates with near-rectangular shapes and straight edges. (c) A continuous γ-SnTe film. (d) A continuous SnTe film with coexisting γ and β phases. The boundaries between the two phases are indicated by the red dashed curves. All the topographic images were acquired at room temperature. The thicknesses of the terraces are indicated by the numbers in units of atomic layers (AL). The areas labeled "s" are bare substrates. The underlined numbers denote the areas in the β phase, while the others are in the γ phase. Setpoints: sample bias voltage $V_s = -0.5$ V and tunneling current $I_t = 5$ pA. [(e) and (f)] Atom resolved topography images of γ- and β-SnTe, respectively. Setpoints: (e) $V_s = -0.2$ V and $I_t = 50$ pA; (f) $V_s = 0.9$ V and $I_t = 100$ pA.

It is difficult to distinguish the two phases from diffraction techniques like RHEED because of the very similar in-plane lattice parameters of these two phases. However, the γ and β phases can be identified from either surface topography or local density of states (see Ref. 13 for details). In most cases, they can easily be recognized from the height of the steps on the surface: 2 AL (6.3 Å) for the γ phase and 1 AL (3.1 Å) for the β phase. In addition, the terrace widths of γ-SnTe are usually several times wider than that of β-SnTe in the same sample [Fig. 2(d)]. The clearest approach to distinguish the two phases is to measure atom resolved images [Figs. 2(e) and 2(f)]: γ-SnTe has a relatively low intrinsic defect density at the surfaces (10^{-10}–10^{-12} cm^{-2}), while that in β-SnTe is several orders of magnitude higher (10^{-13}–10^{-14} cm^{-2}) due to the negative formation energy of Sn vacancies in this phase.[23] The atom resolved image in Fig. 2(f) also agrees well with previous studies of thick SnTe plates, which are confirmed to be in the α or β phase and show Dirac-type surface states.[24]

We have quantitatively studied the evolution of surface topography and the phase distribution of SnTe films as a function of growth conditions. By fixing the flux of SnTe molecules, we reduce the growth control parameters to two: substrate temperature T_{sub} and growth time t_g. Figure 3 shows a series of experiments that vary t_g at certain T_{sub}, and Fig. 4 shows the complementary experiments that fix t_g while changing T_{sub}. In order to perform the statistical analysis, we label the thicknesses of the SnTe terraces in each panel of Figs. 3 and 4. We calculated the total areas of the terraces with specific thicknesses in each sample and extracted three quantities as indicators of growth: (i) the total coverage of SnTe, defined as the total volume of SnTe divided by the total area of the substrate; (ii) the average thickness of SnTe, defined as the total volume of SnTe divided by the area covered by SnTe, i.e., excluding regions of bare substrate; and (iii) the percentage of γ-SnTe, defined as the area of γ-SnTe divided by the total area covered by both γ- and β-SnTe. The results are summarized in Figs. 5 and 7.

At any T_{sub}, the film always starts growing in the γ phase, while it can turn into the β phase when the thickness is larger than 6 AL. In general, the SnTe terraces are larger in the samples grown at higher T_{sub}, for both the γ and β phases. We notice that the total coverage does not increase linearly with t_g, as can be seen from Fig. 5(a). The growth rate at the nucleation stage of deposition is significantly reduced as T_{sub} increases. Once the first 2 AL of SnTe is grown, the film tends to grow at a constant rate.

The control of the nucleation rate is critical in obtaining the desired sample topography. Continuous γ-SnTe films can be grown at $T_{sub} = 90$ °C [Figs. 2(c) and 4(a)], while large and separated plates with regular crystalline shapes can be grown at $T_{sub} = 200$ °C [Figs. 2(b) and 3(j)]. The widths of these nanoplates can be several hundreds of nanometer, and the edges of them are atomically smooth. These nanoplates are ideal model systems to test the theoretical predictions for 2D group-IV monochalcogenide ferroelectric materials.

We have quantitatively analyzed the nucleation process of SnTe on graphene substrates in Fig. 5(b). The explicit nucleation rate I can be fitted by an exponential function $I = A\exp(\Delta E/kT)$, in which k is the Boltzmann constant, $A = (3.59 \pm 0.53) \times 10^{-5}$ μm^{-2} min^{-1} $= (5.99 \pm 0.88) \times 10^{5}$ m^{-2} s^{-1} is a factor that determined by substrate surface conditions and SnTe molecular flux, and $\Delta E = 0.321 \pm 0.005$ eV is the total energy gain on forming a

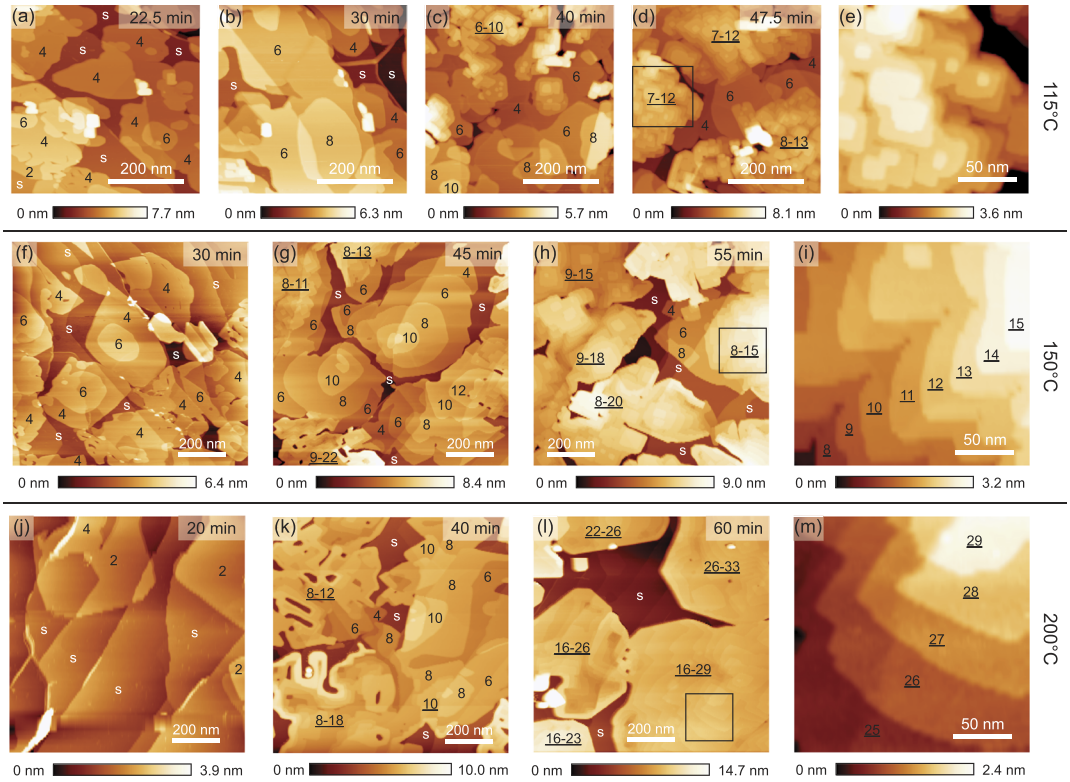

FIG. 3. Evolution of the surface topography with deposition time. The SnTe flux is fixed in all the experiments. The substrate temperature during growth is fixed in each group of images. [(a)–(d)] Samples deposited at 115 °C for 22.5, 30, 40, and 47.5 min, respectively. (e) Magnified image of the area shown by the square outline in (d). [(f)–(h)] Samples deposited at 150 °C for 30, 45, and 55 min, respectively. (i) Magnified image of the area shown by the square outline in (h). [(j)–(l)] Samples deposited at 200 °C for 20, 40, and 60 min, respectively. (m) Magnified image of the area shown by the square outline in (l).

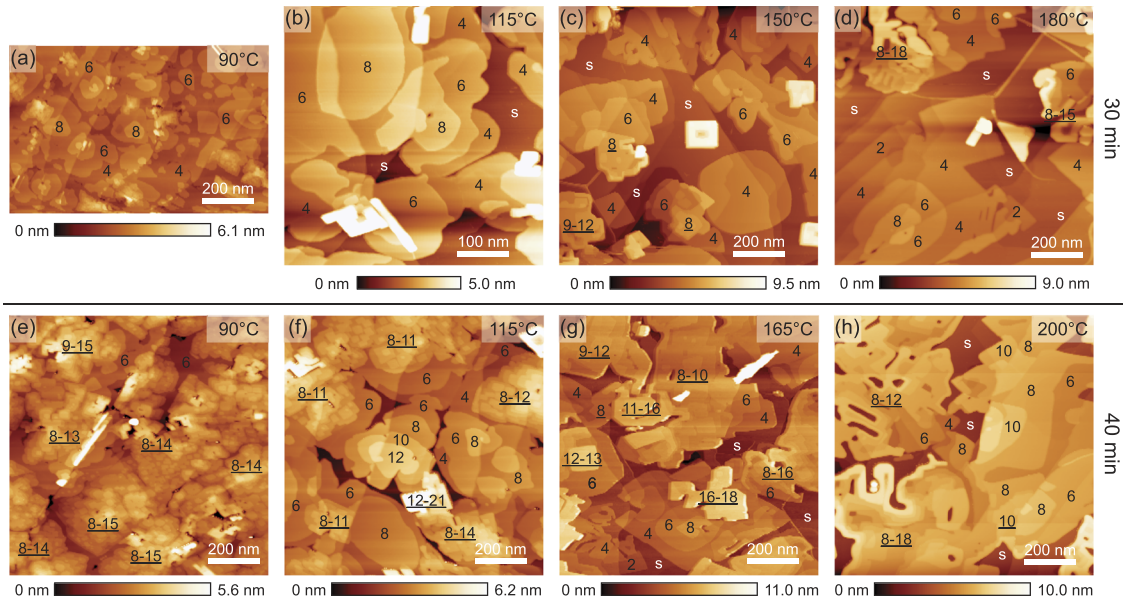

FIG. 4. Evolution of the surface topography with substrate temperature. SnTe flux is fixed in all the experiments. The growth time is fixed in each group of images. [(a)–(d)] Samples deposited for 30 min at 90 °C, 115 °C, 150 °C, and 180 °C, respectively. [(e)–(h)] Samples deposited for 40 min at 90 °C, 115 °C, 165 °C, and 200 °C, respectively.

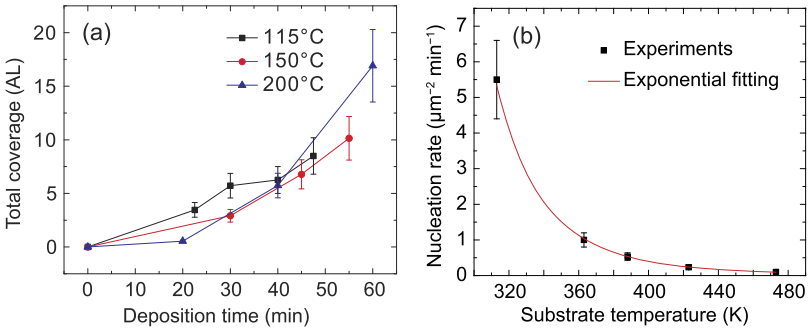

FIG. 5. (a) Dependence of total coverage and deposition time at different substrate temperatures. (b) Substrate temperature dependence of nucleation rate.

nucleus. According to Walton's nucleation theory for small critical nuclei size,[26] the fitting parameters above can be expressed as $A = R(\sigma_{n^*}/a)\left(Ra^2/v\right)^{n^*}$ and $\Delta E = \left(n^*+1\right)Q_{ad} + E_{n^*} - Q_D$, in which R is the rate of impingement of molecules at the substrate surface, n^* are the atoms in a nucleus of critical size, σ_{n^*} is the effective capture width of the critical nucleus for a single atom, a is the separation between absorption sites, v is the frequency of diffusion attempts, Q_{ad} is the binding energy to the surface, E_{n^*} is the net gain in potential energy on forming a cluster of size n^*, and Q_D is the activation energy for surface diffusion. Comparing with the molecule impingement rate, typically $R = 6.2 \times 10^{18}$ m^{-2} s^{-1} or 3.8×10^8 μm^{-2} min^{-1} for a vapor pressure $P = 1 \times 10^{-5}$ mbar at 450 °C, the nucleation rate of SnTe is very slow even on a substrate kept at room temperature. A rough estimation with $a = 0.3$ nm and $v = 1 \times 10^{12}$ s^{-1} yields $Ra^2/v = 5.6 \times 10^{-13}$. If we assume that σ_{n^*} and a are of the same order of magnitude, then $n^* = 1$ is the only reasonable value to obtain the experimental A value. This means that once two SnTe molecules are bonded together, the cluster can continue to grow larger. Therefore, such a slow nucleation rate should be mainly ascribed to the low ΔE.

It should be noted that the quality of a substrate, specifically the concentration and types of defects on its surface, also affects the nucleation rate. For substrates with deep pinholes (depth over 5 nm) or spots that are not sufficiently graphitized, SnTe can easily nucleate at these defects and rapidly grow into tall islands. Figure 6 shows an example of a substrate with some holes that are not covered by graphene, mainly induced by an annealing temperature lower than 1400 °C in the last step of graphene growth. The surface roughness in these holes is higher than the surrounding areas that are sufficiently graphitized, as Fig. 6(b) shows. While graphene lattices can be clearly resolved outside these holes, no atomic resolution is available inside the holes, except from a superstructure corresponding to SiC(0001)—(6 × 6) [Figs. 6(d) and 6(e)]. There are also some low protrusions at the graphene surfaces, which are

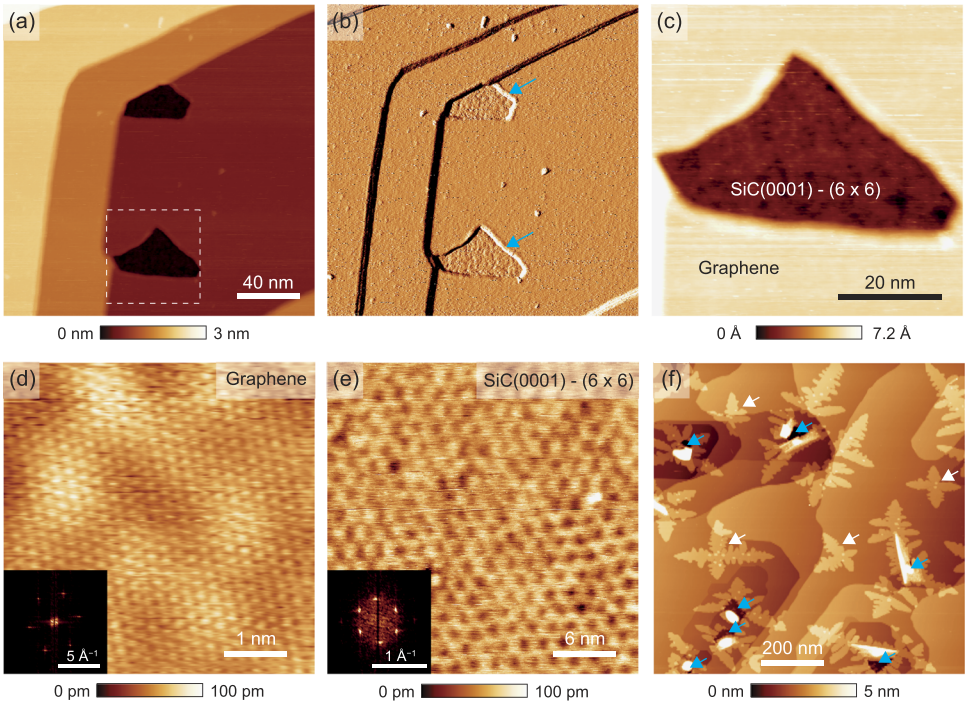

FIG. 6. (a) Topography image of a graphene substrate. $V_s = -0.2$ V and $I_t = 10$ pA. (b) The first-order derivative image of (a). Cyan arrows indicate the areas that are not sufficiently graphitized. (c) Zoom-in image of the area in the dashed square in (a). (d) Atom resolved image of an area covered by graphene. $V_s = 5$ mV and $I_t = 0.5$ nA. Inset: Fourier transformed image of (d). The slight distortion of the hexagonal lattice is induced by thermal drift. (e) Topography image of an area that remains SiC(0001)—(6 × 6). $V_s = -2.0$ V and $I_t = 100$ pA. Inset: Fourier transformed image of (e). (f) A SnTe sample grown on a substrate with SiC(0001)—(6 × 6) areas at room temperature. $V_s = -0.3$ V and $I_t = 2$ pA. The cyan arrows label the islands nucleate at the SiC(0001) - (6 × 6) areas, and the white arrows indicate those nucleate at the other sites on the surface.

considered to be small wrinkles of graphene.[25] A test growth on a defective substrate staying at room temperature shows that most of the nucleation processes happen at these holes [Fig. 6(f)]. SnTe molecules tend to nucleate at the insufficiently graphitized holes unless the substrate temperature is higher than 250 °C. Nucleation on graphene becomes very rare at such a temperature. Therefore, such holes should be avoided during the substrate preparation process.

The distributions of the γ and β phases are summarized in Fig. 7. The primary parameter that determines the structural phase is the thickness of SnTe: the percentage of the γ phase decreases monotonically as the average thickness increases at any given T_{sub}. This trend is also visually reflected in Figs. 3 and 4: all the 2, 4, and 6 AL thick areas are in the γ phase, while very few areas are in the γ phase when the thickness is larger than 10 AL.

Above a thickness of 6 AL, γ-SnTe becomes a metastable phase which coexists and competes with the more stable β phase. Our results also show that thick metastable γ-SnTe has a larger probability to survive when T_{sub} is higher during growth, as Fig. 7 illustrates. At the low T_{sub} end, the percentage of γ-SnTe quickly drops when the thickness is larger than 6 AL; while at the high T_{sub} end, the percentage of γ-SnTe decreases much more slowly as the thickness increases. For instance, when a sample is grown at T_{sub} = 90 °C for 30 min, most of the areas are thinner than 8 AL and are thus in the γ phase [Fig. 4(a)]; an extra 10 min growth at T_{sub} = 90 °C turns most of these areas into the β phase, and there is almost no metastable γ phase in regions thicker than 6 AL [Fig. 4(e)]. On the contrary, many 8 and 10 AL thick γ-SnTe areas can be found in the samples grown at T_{sub} = 150 °C and 200 °C [Figs. 3(g) and 3(k)]. Such a growth mechanism can be possibly rationalized from the perspective of growth dynamics. Since all the SnTe films or plates start to grow in the γ phase, they must overcome a potential barrier to transition into the more stable β phase as the thickness increases above 6 AL. Let us consider the process of adding 2 AL onto a 6 AL thick plate as an example: the most stable structure for 8 AL thick SnTe is the β phase; therefore, if the plate stays in the γ phase, it will experience a strain induced by the lattice anisotropy, which can be characterized by the lattice distortion angle $\Delta\alpha \approx 1 - |\boldsymbol{b}|/|\boldsymbol{c}|$, where $|\boldsymbol{b}|$ and $|\boldsymbol{c}|$ are the lengths of the two in-plane orthorhombic basis

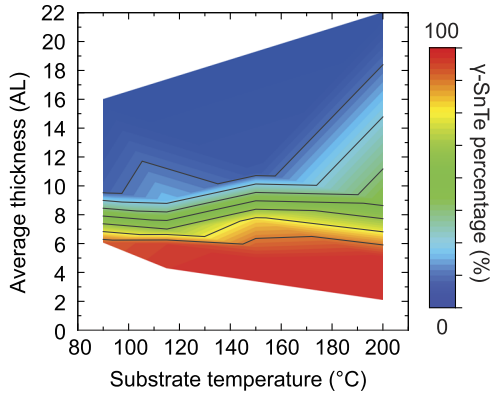

FIG. 7. The percentage of γ-SnTe as a function of average thickness of the SnTe film and the substrate temperature.

of γ-SnTe. Since $\Delta\alpha = 0$ for β-SnTe, a larger $\Delta\alpha$ in metastable γ-SnTe corresponds to a larger strain and thus a larger energy gain. $\Delta\alpha$ decreases monotonically as the temperature increases: for 6 AL γ-SnTe, $\Delta\alpha = 1.6°$ at 27 °C and 1.0° at 117 °C,[13] and is expected to be even smaller at higher temperatures. Therefore, the extra 2 AL SnTe added onto a 6 AL thick γ-SnTe plate will experience less strain at a higher T_{sub} and hence has a higher probability to maintain the γ phase. As the sample is cooled down, the metastable γ phase is quenched, i.e., the strain cannot be released unless sufficient thermal stimulation is applied. This scenario is consistent with the observation that a γ-SnTe plate can occasionally be turned into β-SnTe by annealing at a temperature as low as 360 K.[13]

In conclusion, we have carried out a systematic study of the growth and phase distribution of ultrathin SnTe on graphene substrates. Under different growth conditions, ultrathin SnTe can be grown as either rectangular plates or continuous films. The nucleation rate of SnTe on graphene substrates is found to be highly sensitive to substrate temperature. Thickness is the primary parameter determining which structure is adopted: the layered γ-SnTe is the most stable phase when the thickness is lower than 6 AL, while above 6 AL, it becomes a metastable phase that coexists with the rock salt β-SnTe phase. The substrate temperature during growth is a secondary parameter that affects the phase distribution: the metastable γ phase has a higher probability to survive at a relatively higher substrate temperature. This research paves the way to potential applications based on ultrathin SnTe films, such as novel non-volatile memories and optical-valleytronic devices.

We thank Tianping Ma for providing the MATLAB code that deals with the statistics. This work was financially supported by the Deutsche Forschungsgemeinschaft (DFG, German Research Foundation)—Project No. PA 1812/2-1.

REFERENCES

[1] C. Cui, F. Xue, W.-J. Hu, and L.-J. Li, "Two-dimensional materials with piezoelectric and ferroelectric functionalities," npj 2D Mater. Appl. **2**, 18 (2018).
[2] R. Fei, W. Li, J. Li, and L. Yang, "Giant piezoelectricity of monolayer group IV monochalcogenides: SnSe, SnS, GeSe, and GeS," Appl. Phys. Lett. **107**, 173104 (2015).
[3] P. Z. Hanakata, A. Carvalho, D. K. Campbell, and H. S. Park, "Polarization and valley switching in monolayer group-IV monochalcogenides," Phys. Rev. B **94**, 035304 (2016).
[4] M. Mehboudi, B. M. Fregoso, Y. Yang, W. Zhu, A. van der Zande, J. Ferrer, L. Bellaiche, P. Kumar, and S. Barraza-Lopez, "Structural phase transition and material properties of few-layer monochalcogenides," Phys. Rev. Lett. **117**, 246802 (2016).
[5] R. X. Fei, W. Kang, and L. Yang, "Ferroelectricity and phase transitions in monolayer group-IV monochalcogenides," Phys. Rev. Lett. **117**, 097601 (2016).
[6] M. Wu and X. C. Zeng, "Intrinsic ferroelasticity and/or multiferroicity in two-dimensional phosphorene and phosphorene analogues," Nano Lett. **16**, 3236 (2016).
[7] H. Wang and X. F. Qian, "Two-dimensional multiferroics in monolayer group IV monochalcogenides," 2D Mater. **4**, 015042 (2017).
[8] D. Xiao, G.-B. Liu, W. Feng, X. Xu, and W. Yao, "Coupled spin and valley physics in monolayers of MoS_2 and other group-VI dichalcogenides," Phys. Rev. Lett. **108**, 196802 (2012).
[9] A. Castellanos-Gomez, "Black phosphorous: Narrow gap, wide applications," J. Phys. Chem. Lett. **6**, 4280 (2015).
[10] S. N. Dutta and G. A. Jeffery, "On the structure of germanium selenide and related binary IV/VI compounds," Inorg. Chem. **4**, 1363 (1965).

[11] K. Chang, J. Liu, H. Lin, N. Wang, K. Zhao, A. Zhang, F. Jin, Y. Zhong, X. Hu, W. Duan, Q. Zhang, L. Fu, Q.-K. Xue, X. Chen, and S.-H. Ji, "Discovery of robust in-plane ferroelectricity in atomic-thick SnTe," Science **353**, 274 (2016).
[12] K. L. I. Kobayashi, Y. Kato, Y. Katayama, and K. F. Komatsubara, "Carrier-concentration-dependent phase transition in SnTe," Phys. Rev. Lett. **37**, 772 (1976).
[13] K. Chang, T. P. Kaloni, H. Lin, A. Bedoya-Pinto, A. K. Pandeya, I. Kostanovskiy, K. Zhao, Y. Zhong, X. Hu, Q.-K. Xue, X. Chen, S.-H. Ji, S. Barraza-Lopez, and S. S. P. Parkin, "Enhanced spontaneous polarization in ultrathin SnTe films with layered antipolar structure," Adv. Mater. **31**, 1804428 (2019).
[14] T. H. Hsieh, H. Lin, J. Liu, W. Duan, A. Bansil, and L. Fu, "Topological crystalline insulators in the SnTe material class," Nat. Commun. **3**, 982 (2012).
[15] Y. Tanaka, Z. Ren, T. Sato, K. Nakayama, S. Souma, T. Takahashi, K. Segawa, and Y. Ando, "Experimental realization of a topological crystalline insulator in SnTe," Nat. Phys. **8**, 800 (2012).
[16] S. Y. Xu, C. Liu, N. Alidoust, M. Neupane, D. Qian, I. Belopolski, J. D. Denlinger, Y. J. Wang, H. Lin, L. A. Wray, G. Landolt, B. Slomski, J. H. Dil, A. Marcinkova, E. Morosan, Q. Gibson, R. Sankar, F. C. Chou, R. J. Cava, A. Bansil, and M. Z. Hasan, "Observation of a topological crystalline insulator phase and topological phase transition in $Pb_{1-x}Sn_xTe$," Nat. Commun. **3**, 1192 (2012).
[17] P. Dziawa, B. J. Kowalski, K. Dybko, R. Buczko, A. Szczerbakow, M. Szot, E. Lusakowska, T. Balasubramanian, B. M. Wojek, M. H. Berntsen, O. Tjernberg, and T. Story, "Topological crystalline insulator states in $Pb_{1-x}Sn_xSe$," Nat. Mater. **11**, 1023 (2012).
[18] A. Kozbial, Z. Li, C. Conaway, R. McGinley, S. Dhingra, V. Vahdat, F. Zhou, B. D'Urso, H. Liu, and L. Li, "Study on the surface energy of graphene by contact angle measurements," Langmuir **30**, 8598 (2014).
[19] Y. P. Jia, L. W. Guo, J. J. Lin, L. L. Chen, and X. L. Chen, "Wafer-scale graphene on 2 inch SiC with uniform structural and electrical characteristics," Chin. Sci. Bull. **57**, 3022 (2012).
[20] J. Hass, W. A. de Heer, and E. H. Conrad, "The growth and morphology of epitaxial multilayer graphene," J. Phys.: Condens. Matter **20**, 323202 (2008).
[21] Q. Wang, W. Zhang, L. Wang, K. He, X. Ma, and Q. Xue, "Large-scale uniform bilayer graphene prepared by vacuum graphitization of 6H-SiC(0001) substrates," J. Phys.: Condens. Matter **25**, 095002 (2013).
[22] R. F. Brebrick, "Composition stability limits for the rocksalt-structure phase $(Pb_{1-y}Sn_y)_{1-x}Te_x$ from lattice parameter measurements," J. Phys. Chem. Solids **32**, 551 (1971).
[23] N. Wang, D. West, J. Liu, J. Li, Q. Yan, B.-L. Gu, S. B. Zhang, and W. Duan, "Microscopic origin of the p-type conductivity of the topological crystalline insulator SnTe and the effect of Pb alloying," Phys. Rev. B **89**, 045142 (2014).
[24] D. Zhang, H. Baek, J. Ha, T. Zhang, J. Wyrick, A. V. Davydov, Y. Kuk, and J. A. Stroscio, "Quasiparticle scattering from topological crystalline insulator SnTe(001) surface states," Phys. Rev. B **89**, 245445 (2014).
[25] G. F. Sun, J. F. Jia, Q. K. Xue, and L. Li, "Atomic-scale imaging and manipulation of ridges on epitaxial graphene on 6H-SiC(0001)," Nanotechnology **20**, 355701 (2009).
[26] D. Walton, "Nucleation of vapor deposits," J. Chem. Phys. **37**, 2182 (1962).